Human Molecular Genetics, 2009, Vol. 18, No. 11 **2001–2013**
doi:10.1093/hmg/ddp124
Advance Access published on March 16, 2009

Genetic interaction between the *m*-AAA protease isoenzymes reveals novel roles in cerebellar degeneration

Paola Martinelli[1], Veronica La Mattina[1], Andrea Bernacchia[1], Raffaella Magnoni[2], Federica Cerri[3], Gregory Cox[4], Angelo Quattrini[3], Giorgio Casari[2,5] and Elena I. Rugarli[1,6,*]

[1]Division of Biochemistry and Genetics, Istituto Neurologico 'C. Besta', Milan, Italy, [2]Human Molecular Genetics Unit, San Raffaele Scientific Institute, Milan, Italy, [3]Institute of Experimental Neurology and Division of Neuroscience, San Raffaele Scientific Institute, Milan, Italy, [4]The Jackson Laboratory, Bar Harbor, ME 04609, USA, [5]Vita-Salute San Raffaele University, School of Medicine, Milan, Italy and [6]Department of Neuroscience and Medical Biotechnologies, University of Milano-Bicocca, Milan, Italy

Received February 9, 2009; Revised March 5, 2009; Accepted March 12, 2009

The mitochondrial *m*-AAA protease has a crucial role in axonal development and maintenance. Human mitochondria possess two *m*-AAA protease isoenzymes: a hetero-oligomeric complex, composed of paraplegin and AFG3L2 (Afg3 like 2), and a homo-oligomeric AFG3L2 complex. Loss of function of paraplegin (encoded by the *SPG7* gene) causes hereditary spastic paraplegia, a disease characterized by retrograde degeneration of cortical motor axons. *Spg7*$^{-/-}$ mice show a late-onset degeneration of long spinal and peripheral axons with accumulation of abnormal mitochondria. In contrast, *Afg3l2*$^{Emv66/Emv66}$ mutant mice, lacking the AFG3L2 protein, are affected by a severe neuromuscular phenotype, due to defects in motor axon development. The role of the homo-oligomeric *m*-AAA protease and the extent of cooperation and redundancy between the two isoenzymes in adult neurons are still unclear. Here we report an early-onset severe neurological phenotype in *Spg7*$^{-/-}$ *Afg3l2*$^{Emv66/+}$ mice, characterized by loss of balance, tremor and ataxia. *Spg7*$^{-/-}$ *Afg3l2*$^{Emv66/+}$ mice display acceleration and worsening of the axonopathy observed in paraplegin-deficient mice. In addition, they show prominent cerebellar degeneration with loss of Purkinje cells and parallel fibers, and reactive astrogliosis. Mitochondria from affected tissues are prone to lose mt-DNA and have unstable respiratory complexes. At late stages, neurons contain structural abnormal mitochondria defective in COX-SDH reaction. Our data demonstrate genetic interaction between the *m*-AAA isoenzymes and suggest that different neuronal populations have variable thresholds of susceptibility to reduced levels of the *m*-AAA protease. Moreover, they implicate impaired mitochondrial proteolysis as a novel pathway in cerebellar degeneration.

INTRODUCTION

Mitochondrial dysfunction is involved in several neurodegenerative diseases, including hereditary spastic paraplegia (HSP) (1,2). HSP is a genetic disease characterized by weakness, spasticity and loss of the vibratory sense in the lower limbs, owing to retrograde degeneration of the long axons of the corticospinal tracts and the fasciculus gracilis (3,4). A fraction (5–10%) of autosomal recessive cases of HSP are due to mutations in *SPG7*, encoding paraplegin (5–7). Paraplegin is one component of the *m*-AAA protease, a high molecular weight complex in the inner mitochondrial membrane evolutionary conserved from yeast to mammals. The human *m*-AAA protease exists in a hetero-oligomeric form, composed of paraplegin and AFG3L2 (Afg3 like 2), and in a

*To whom correspondence should be addressed at: Division of Biochemistry and Genetics, Istituto Neurologico 'C. Besta', via Temolo 4 20126, Milano, Italy. Tel: +39 0223942614; Fax: +39 0223942619; Email: rugarli@istituto-besta.it; elena.rugarli@unimib.it

homo-oligomeric complex containing only AFG3L2 (8). Mice contain an additional protein, AFG3L1, which is highly homologous to AFG3L2, and is also capable of homo-oligomerizing and interacting with paraplegin (8,9). *AFG3L1* is a pseudogene in humans (9).

Studies in yeast, which harbors only a hetero-oligomeric proteolytic complex, have shown that the *m*-AAA protease performs house-keeping functions, by degrading unassembled components of the respiratory complexes and misfolded inner membrane proteins, and by mediating the proteolytic maturation of specific substrates (10). Among these is MrpL32, a component of the large subunit of the mitochondrial ribosome, explaining why yeast cells depleted of the protease show defective mitochondrial protein synthesis (11). Both the hetero-oligomeric and the homo-oligomeric mammalian isoenzymes are able to rescue phenotypes of yeast cells depleted of the *m*-AAA protease (8).

Although the different subunits of the mammalian *m*-AAA protease seem to be largely redundant, they reveal substantial tissue-specific differences (8). The murine AFG3L2 is much more abundant in the brain than paraplegin and AFG3L1 (8). The different expression pattern and the ability to homo-oligomerize and/or hetero-oligomerize underlie the dramatic difference in phenotype of *Spg7* and *Afg3l2* mouse mutants. Paraplegin-deficient mice display an impaired motor performance at the rotarod test at 4 months of age and a slowly progressive distal axonopathy of long motor and sensory axons in the spinal cord starting at about 7 months of age, reproducing the late-onset phenotype of human HSP patients (12). Paraplegin-deficient axons accumulate abnormal gigantic mitochondria with disrupted cristae in their distal ends long before swelling and degeneration (12). This suggests that the AFG3L2 homo-complex is sufficient for axonal development and for the maintenance of axonal integrity in adult life, with the exception of long central and peripheral axons during aging. In contrast, two different mouse mutants harboring mutations in *Afg3l2* on both alleles (the *paralysé* spontaneous mutant and the $Afg3l2^{Emv66/Emv66}$ mutant) display a severe phenotype, beginning at P7 with hindlimb paraparesis and leading to death at around P16. This is characterized by a defect in axonal development with delayed myelination and impaired axonal radial growth in the central and peripheral nervous systems (13). The severity of the phenotype hampers the evaluation of a possible role of the homo-oligomeric AFG3L2 *m*-AAA isoenzyme in axonal degeneration. In addition, the question whether the hetero-oligomeric and the homo-oligomeric complexes are functionally equivalent or have specific roles in different neurons is still unanswered.

By generating mice carrying different dosages of AFG3L2 and paraplegin, we now provide evidence that the homo-oligomeric and hetero-oligomeric *m*-AAA isoenzymes are largely redundant in adult neurons and attribute to the global dosage of the *m*-AAA protease an important role to prevent neurodegeneration in various brain areas. Notably, we find that $Spg7^{-/-}$ $Afg3l2^{Emv66/+}$ double mutants show an early-onset ataxic phenotype, indicating a novel unexpected role of the *m*-AAA proteases in cerebellar degeneration.

RESULTS

Severe neurological phenotype in $Spg7^{-/-}$ $Afg3l2^{Emv66/+}$ double mutants

To obtain mice with different dosages of paraplegin and AFG3L2, we crossed two lines carrying loss-of-function mutations in the *Spg7* and *Afg3l2* genes: the paraplegin-deficient $Spg7^{-/-}$ line, previously generated by gene targeting (12), and the $Afg3l2^{Emv66/+}$ mutants (13). The $Afg3l2^{Emv66}$ allele arose after a novel ecotropic murine leukemia proviral reinsertion in intron 14 of the *Afg3l2* gene and does not produce the AFG3L2 protein (13). $Afg3l2^{Emv66/+}$ mice show normal fertility and appearance (13). Double-heterozygous lines from the initial crossing were intercrossed to obtain mice with different genotypes. To answer the question whether the homo-oligomeric AFG3L2 *m*-AAA protease has redundant or cooperative functions with the hetero-oligomeric paraplegin/AFG3L2 *m*-AAA complex in adult neurons, we focused on mice carrying only one functional allele of *Afg3l2* in combination with different dosages of paraplegin.

$Spg7^{+/+}$ $Afg3l2^{Emv66/+}$, $Spg7^{+/-}$ $Afg3l2^{Emv66/+}$ and $Spg7^{-/-}$ $Afg3l2^{Emv66/+}$ mice were all born at the expected Mendelian ratio and were indistinguishable from wild-type littermates at birth. However, at about 6 weeks of age, $Spg7^{-/-}$ $Afg3l2^{Emv66/+}$ mice showed reduced cage activity and altered coordination of the hindlimbs during gait, allowing their recognition in the cage. The neurological phenotype progressed rapidly such that by 9 weeks of age, there was a clear loss of balance, frank uncoordinated gait, tremor and dystonic movements of the head, being highly suggestive of ataxia (Supplementary Material, Movies). Moreover, $Spg7^{-/-}$ $Afg3l2^{Emv66/+}$ mice lost weight beginning at 9 weeks, developed a prominent kyphosis and ultimately appeared cachexic (Fig. 1A and D). The median age of survival of $Spg7^{-/-}$ $Afg3l2^{Emv66/+}$ mice was 13 weeks and they never lived longer than 20 weeks (Fig. 1B).

To identify more precisely the time of onset of the motor impairment, we performed accelerating rotarod tests at different ages, comparing the performance of mice carrying different combinations of *Afg3l2* and *Spg7* alleles. $Spg7^{-/-}$ $Afg3l2^{Emv66/+}$ mice began to show obvious motor abnormalities at 7 weeks (Fig. 1C). The motor ability rapidly worsened (Fig. 1C), and at 11 weeks, most $Spg7^{-/-}$ $Afg3l2^{Emv66/+}$ mice were unable to stand on the rod. $Spg7^{-/-}$, single *Afg3l2* heterozygous or double *Spg7*/*Afg3l2* heterozygous mice performed the rotarod test like wild-type controls (Fig. 1C; Supplementary Material, Fig. S1). Consistently, we previously found that motor impairment of $Spg7^{-/-}$ mice can be first detected with the rotarod test at about 18 weeks (12). These data suggest that halving the dosage of *Afg3l2* in an *Spg7* null background results in a remarkable early onset and rapidly progressing ataxic phenotype.

$Spg7^{-/-}$ $Afg3l2^{Emv66/+}$ mice show an acceleration of the axonopathy of paraplegin-deficient mice

As a first step to investigate the cause of the neurological phenotype of $Spg7^{-/-}$ $Afg3l2^{Emv66/+}$ mice, we assessed whether these animals show the same neuropathological abnormalities

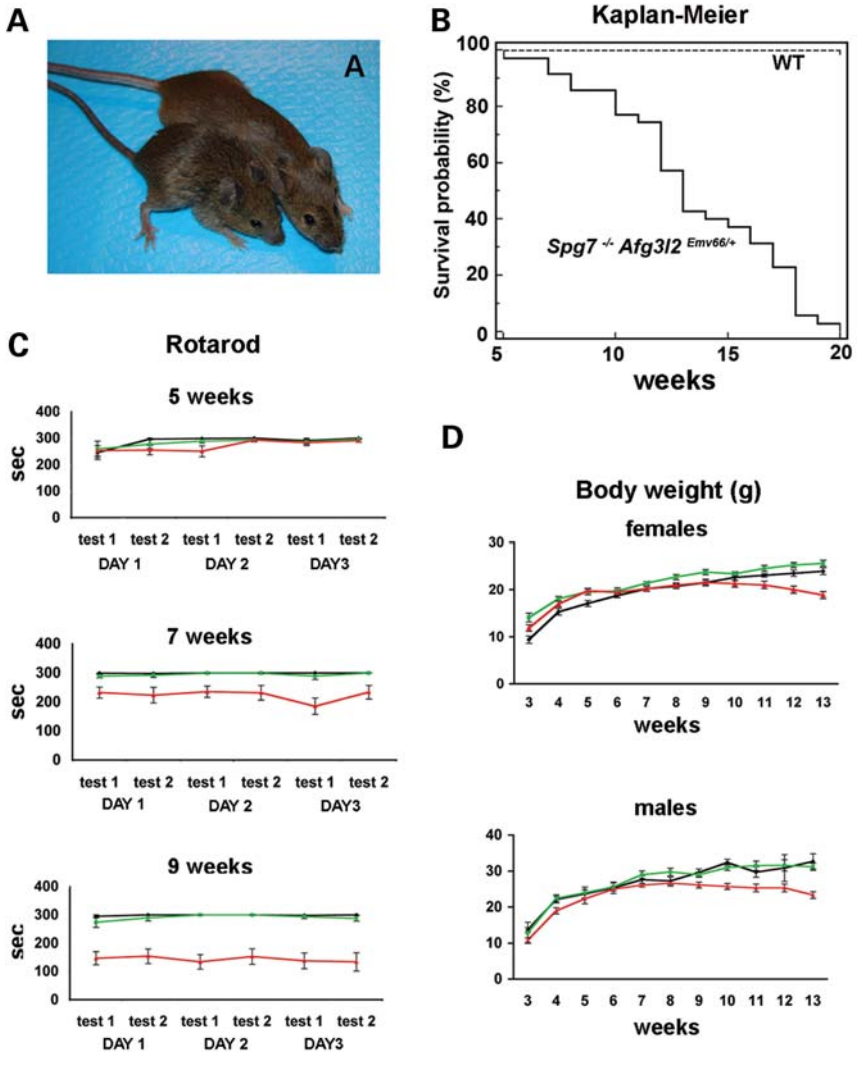

Figure 1. An early-onset neurological phenotype in $Spg7^{-/-}$ $Afg3l2^{Emv66/+}$ double mutants. (**A**) A 13-week-old $Spg7^{-/-}$ $Afg3l2^{Emv66/+}$ mouse (on the left) compared with a wild-type littermate (on right). Note the loss of weight, the kyphosis and abnormal posture of the hindlimbs. (**B**) Kaplan–Meier survival curve of $Spg7^{-/-}$ $Afg3l2^{Emv66/+}$ mice ($n = 38$) compared with wild-type ($n = 27$) shows that they never survive longer than 20 weeks of age ($P < 0.0001$, log-rank test). (**C**) Accelerating rotarod tests of wild-type (black, $n = 8$), $Spg7^{-/-}$ (green, $n = 7$) and $Spg7^{-/-}$ $Afg3l2^{Emv66/+}$ mice (red, $n = 16$) indicate normal motor performance of $Spg7^{-/-}$ $Afg3l2^{Emv66/+}$ at 5 weeks, the beginning of a motor impairment at 7 weeks and a dramatic phenotype at 9 weeks (error bars are SEM; Student's *t*-test: $P < 0.001$ at each test). (**D**) Weight curves of female and male wild-type ($n \geq 7$, black), $Spg7^{-/-}$ ($n \geq 7$, green) and $Spg7^{-/-}$ $Afg3l2^{Emv66/+}$ mice ($n \geq 7$, red). Error bars are SEM.

as paraplegin-deficient mice, but with an earlier age of onset and increased severity. In $Spg7^{-/-}$ mice, axonal swellings and degenerating fibers were previously detected in the antero-lateral funiculi of the spinal cord at lumbar levels, where the distal axons of the rubro-spinal, vestibulo-spinal and reticulo-spinal tracts descend, starting at about 8 months (12). As expected, we found neither signs of axonopathy nor accumulation of abnormal mitochondria in axons of paraplegin-deficient mice at 13 weeks of age (Fig. 2B and E). In contrast, axonal swellings were already observed in the spinal cord of $Spg7^{-/-}$ $Afg3l2^{Emv66/+}$ mice (Fig. 2C). Ultrastructural studies showed that a large number of axons located in the antero-lateral columns of the lumbar spinal cord accumulated abnormal enlarged mitochondria, characterized by vesicular and degenerating cristae (Table 1 and Fig. 2F). Some swollen axons contained a massive accumulation of neurofilaments, suggestive of impaired axonal transport (data not shown).

The peripheral nerve in $Spg7^{-/-}$ mice is involved by axonopathic changes at about 10 months and by frank degeneration after 16 months of age (12). Ultrastructural studies showed that a large percentage of sciatic nerve axons accumulate abnormal enlarged mitochondria in $Spg7^{-/-}$ $Afg3l2^{Emv66/+}$ mice already at 13 weeks (Fig. 2I and Table 1).

In conclusion, these data reveal that the homo-oligomeric AFG3L2 *m*-AAA protease partially compensates for the loss of the hetero-oligomeric paraplegin-containing complex in the spinal cord and sciatic nerve at least in young animals, thus proving *in vivo* that the two isoenzymes are largely redundant.

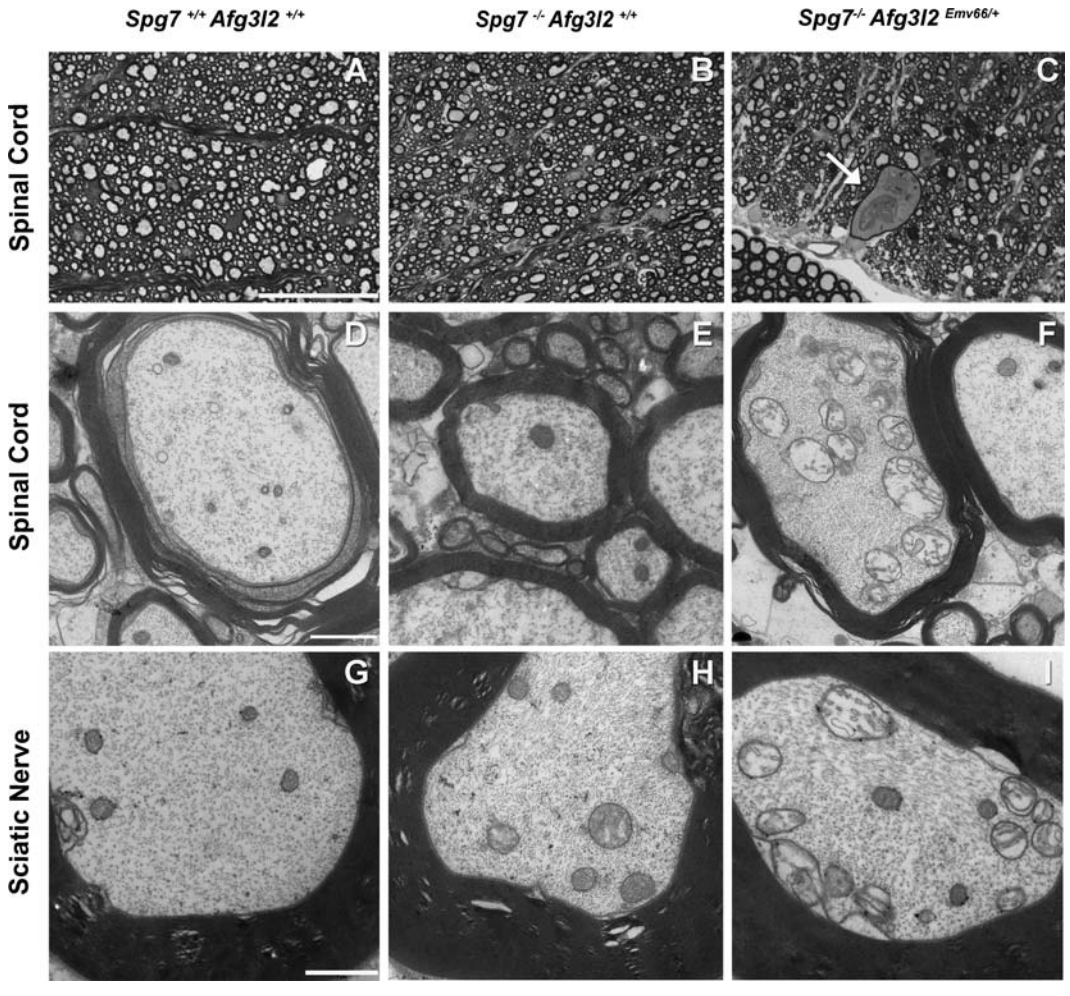

Figure 2. *Spg7*$^{-/-}$ *Afg3l2*$^{Emv66/+}$ mice show distal spinal and peripheral axonopathy at 13 weeks. (**A**–**C**) Semithin transverse sections of the lumbar part of the spinal cord of *Spg7*$^{-/-}$ *Afg3l2*$^{Emv66/+}$ mice show prominent axonal swelling already at 13 weeks (C, arrow). At this age, no phenotype is detected in paraplegin-deficient mice (B). (**D**–**F**) Ultrathin sections confirm the presence of several axons containing swollen mitochondria with abnormally organized membrane compartments in *Spg7*$^{-/-}$ *Afg3l2*$^{Emv66/+}$ (F). Mitochondrial cristae appear lost, swollen or tubular in morphology (F). (**G**–**I**) Ultrastructural studies of distal sciatic nerve confirm the presence of axons containing abnormal swollen mitochondria already at this age only in *Spg7*$^{-/-}$ *Afg3l2*$^{Emv66/+}$ (I). Bars: 50 μm in A–C, 1 μm in D–I.

The *m*-AAA protease is involved in cerebellar degeneration

The ataxic features of *Spg7*$^{-/-}$ *Afg3l2*$^{Emv66/+}$ mice strongly point to cerebellar dysfunction. Nissl-stained sections of the cerebellum showed a comparable number of Purkinje cells in *Spg7*$^{-/-}$ *Afg3l2*$^{Emv66/+}$ mice and wild-type littermates at 7 weeks of age (lobule III counts: 148.3 ± 35.2 Purkinje cells in *Spg7*$^{-/-}$ *Afg3l2*$^{Emv66/+}$ mice versus 142.3 ± 15.3 in wild-types), whereas at 13 weeks, loss of neurons became apparent in the mutants (lobule III counts: 115.5 ± 21.7 Purkinje cells in *Spg7*$^{-/-}$ *Afg3l2*$^{Emv66/+}$ mice versus 161.3 ± 6.7 in wild-types, $P < 0.02$ in *t*-test). Semithin sections of the cerebellum showed that Purkinje cell bodies and dendrites accumulated abnormal vacuolar structures already at 7 weeks of age (Table 2) and more conspicuously at 13 weeks, when these alterations had progressed to frank signs of neuronal degeneration (Table 2; Fig. 3B). Several Purkinje cells had a dark, shrunken appearance with nuclei characterized by irregular membranes (Fig. 3B). Purkinje cells project through the molecular layer of the cerebellum an elaborate dendritic tree that can be selectively marked with antibodies against the calcium-binding protein calbindin. Calbindin immunohistochemistry showed mild abnormalities at 7 weeks and a prominent loss of Purkinje cell dendrites at 13 weeks in *Spg7*$^{-/-}$ *Afg3l2*$^{Emv66/+}$ mice (Fig. 3D; Supplementary Material, Fig. S2). Purkinje cells that still cross-reacted with the calbindin antibody had a less ramified dendritic tree, composed of shorter and thicker branches (Fig. 3D).

Granule cells are located deep into the Purkinje cell layer, and project into the molecular layer, where their axons split in two branches that take diametrically opposite directions forming the shape of a T (hence the name of parallel fibers). Purkinje cell dendrites make synaptic contacts with parallel fibers, whereas their axons extend out thorough the granule cell layer to the white matter. To determine whether cerebellar axons are lost in the double mutants, we stained sections with an antibody against a phosphorylated form of neurofilament

Table 1. Quantification of axons containing abnormal swollen mitochondria in the spinal cord and sciatic nerve

Genotype	*n*	%Fibers with abnormal mitochondria	Fibers scored
Lumbar spinal cord			
Spg7$^{+/+}$ *Afg3l2*$^{+/+}$	2	1 ± 0.1	560
Spg7$^{-/-}$ *Afg3l2*$^{+/+}$	3	2.2 ± 0.9	574
Spg7$^{-/-}$ *Afg3l2*$^{Emv66/+}$	3	24.6 ± 1.9*	494
Distal sciatic nerve			
Spg7$^{+/+}$ *Afg3l2*$^{+/+}$	3	1.2 ± 1	210
Spg7$^{-/-}$ *Afg3l2*$^{+/+}$	3	6.4 ± 0.8	171
Spg7$^{-/-}$ *Afg3l2*$^{Emv66/+}$	3	39.9 ± 5**	136

Student's *t*-test, *Spg7*$^{-/-}$ *Afg3l2*$^{Emv66/+}$ versus *Spg7*$^{-/-}$ *Afg3l2*$^{+/+}$: $^{*}P = 0.000052$; $^{**}P = 0.0004$.

Table 2. Quantification of abnormal, vacuolated Purkinje cells in the cerebella of mice with different dosages of AFG3L2 and paraplegin

Genotype	Age (weeks)	*n*	%Purkinje cells with abnormal morphology	Cells scored
Spg7$^{+/+}$ *Afg3l2*$^{+/+}$	13	3	0.99 ± 0.48	665
Spg7$^{+/+}$ *Afg3l2*$^{Emv66/+}$	13	3	3.2 ± 1.7	1022
Spg7$^{-/-}$ *Afg3l2*$^{+/+}$	13	3	8.4 ± 5	821
Spg7$^{+/-}$ *Afg3l2*$^{Emv66/+}$	13	3	8.7 ± 7.8	1052
Spg7$^{-/-}$ *Afg3l2*$^{Emv66/+}$	7	3	10.9 ± 3.44	789
Spg7$^{-/-}$ *Afg3l2*$^{Emv66/+}$	13	3	41.3 ± 10.3*	474

Student's *t*-test, *Spg7*$^{-/-}$ *Afg3l2*$^{Emv66/+}$ versus *Spg7*$^{+/+}$ *Afg3l2*$^{+/+}$: $^{*}P = 0.02$.

(SMI31), specifically enriched in axons. The molecular layer appeared normal at 7 weeks, but was characteristically depleted of parallel fibers at 13 weeks in *Spg7*$^{-/-}$ *Afg3l2*$^{Emv66/+}$ mice (Fig. 3F; Supplementary Material, Fig. S2). High-magnification microscopic analysis disclosed the presence of several axons containing swellings at their ends (Supplementary Material, Fig. S3). Significant loss of axons was also detected at 13 weeks in the granule cell layer, containing both cerebellar afferents and efferents (Fig. 3H). TUNEL assay did not disclose significant apoptosis in any cerebellar layer (Supplementary Material, Fig. S4), although extensive and pronounced reactive astrogliosis was found in the granular cell layer (Fig. 3J). None of these alterations was detected in paraplegin-deficient, *Afg3l2* heterozygous, *Spg7/Afg3l2* double-heterozygous or wild-type littermates at the same age (Supplementary Material, Fig. S5; data not shown). However, when analyzed in semithin sections, *Spg7*$^{-/-}$ mice and also double-heterozygous mice showed a slight increase of vacuolated Purkinje cells compared with wild-type mice at 13 weeks, although these cells never displayed prominent degenerative features at this age (Table 2; Supplementary Material, Fig. S5).

Previous studies showed a comparable number of Purkinje cells in the cerebella of homozygous *Afg3l2*$^{Emv66/Emv6}$ (6) mice and wild-type littermates, indicating a normal migration of Purkinje cells during early development (13). These data raise the question as to whether the development of Purkinje cell dendrites, which occurs after birth in the mouse, proceeds normally in the absence of AFG3L2. We analyzed Purkinje cell dendrite development by performing calbindin immunohistochemistry at postnatal days (P) 7 and 14. In

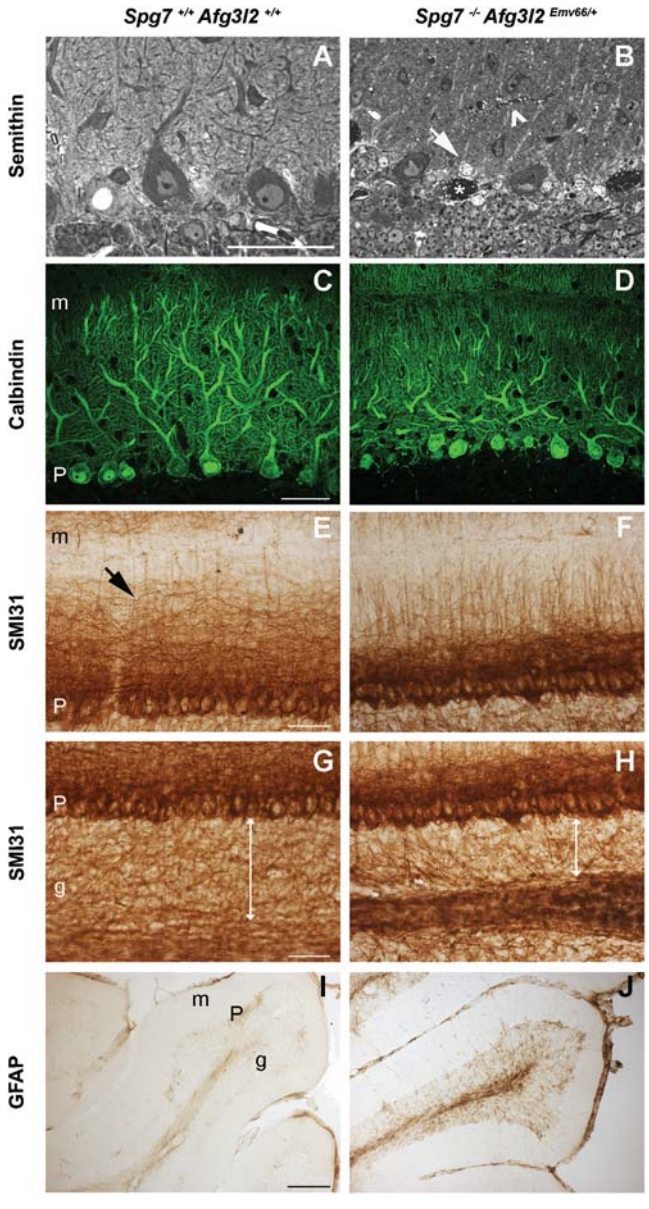

Figure 3. Cerebellar degeneration in *Spg7*$^{-/-}$ *Afg3l2*$^{Emv66/+}$ mice. (**A** and **B**) Semithin sections across the cerebellum of WT and *Spg7*$^{-/-}$ *Afg3l2*$^{Emv66/+}$ mice show abnormal vacuolated Purkinje cell bodies (asterisks) and dendrites (arrowhead) at 13 weeks in the mutants (B). In many areas, Purkinje cells presented dark degenerative appearance, and at the interface between the molecular and granular layers, there are numerous cell bodies of the Bergmann glia, identified by their pale nucleus with few masses of heterochromatin in a rim below the nuclear envelope (B, arrows). (**C** and **D**) Purkinje cells are stained with an anti-calbindin antibody. A drastic reduction of the dendritic tree of residual Purkinje cells is evident in *Spg7*$^{-/-}$ *Afg3l2*$^{Emv66/+}$ mice at 13 weeks of age (D). Dendrites appear less ramified and complex (D). (**E**–**H**) Immunohistochemistry of cerebellar sections with SMI31 antibody. In the molecular layer, parallel fibers (arrow in E) are characteristically lost (F). The granule cell layer appears reduced in thickness and depleted of axons in *Spg7*$^{-/-}$ *Afg3l2*$^{Emv66/+}$ (H). (**I** and **J**) Reactive astrogliosis is detected in the granule cell layer with an anti-GFAP antibody in *Spg7*$^{-/-}$ *Afg3l2*$^{Emv66/+}$ (J). Bars: 50 μm in A–H; 200 μm in I–J. m, molecular layer; P, Purkinje cell layer; g, granule cell layer.

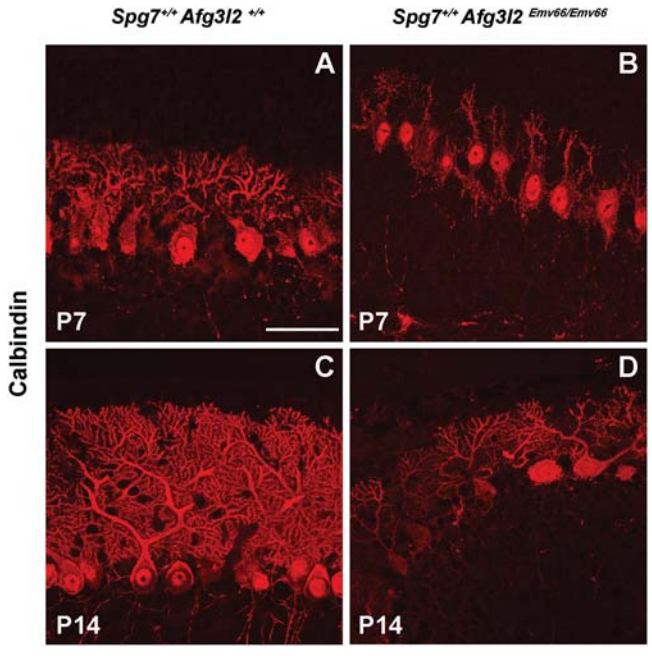

Figure 4. Abnormal Purkinje cell dendritogenesis in AFG3L2-deficient mice. Calbindin staining of the developing dendritic tree of Purkinje cells in WT animals at P7 (**A**) and P14 (**C**). In *Afg3l2*$^{Emv66/Emv66}$ mice, dendritogenesis is strongly impaired (**B** and **D**). At P7, the Purkinje cells have migrated to their position, but still retain bipolar morphology and fail to develop dendrites (B). Dendrites are still largely underdeveloped at P14 (D). Bar: 50 μm.

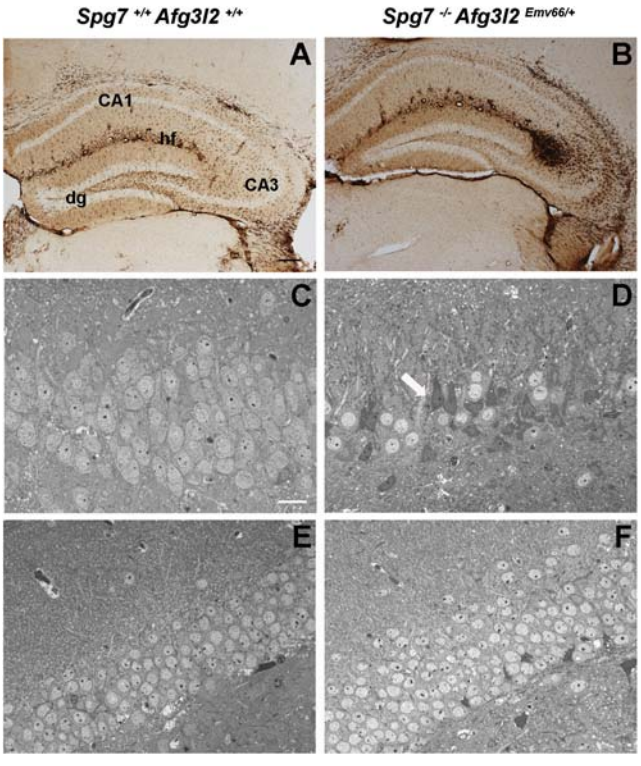

Figure 5. Degeneration of hippocampal CA3 pyramidal neurons. (**A** and **B**) Reactive astrogliosis is detected in the hippocampus with an anti-GFAP antibody in the lacunosum-moleculare and radial layers of the CA3 field, deep into the hippocampal fissure (hf), in *Spg7*$^{-/-}$ *Afg3l2*$^{Emv66/+}$ mice at 13 weeks of age (B). (**C** and **D**) Semithin sections across the pyramidal layer of the CA3 field reveal loss of neuron and degenerative features in the *Spg7*$^{-/-}$ *Afg3l2*$^{Emv66/+}$ mice (D, arrow). (**E** and **F**) Granule neurons of the dentate gyrus appear normal in both genotypes. Bars: 200 μm in A–B; 20 μm in C–F. hf, hippocampal fissure; dg, dentate gyrus; CA1, CA1 field; CA3, CA3 field.

wild-type mice, Purkinje cells extended an apical dendrite that started to ramify in secondary dendrites already at P7, and by P14 had attained a remarkable growth of their dendritic arborization (Fig. 4A and C). In contrast, in *Afg3l2*$^{Emv66/Emv66}$ mice, most Purkinje cells at P7 still retained the bipolar fusiform shape that is typical of these neurons during their migration (14), and at P14 showed a drastic impairment in the progression of the dendritic tree maturation (Fig. 4B and D).

In conclusion, these data demonstrate for the first time an important role of the mitochondrial *m*-AAA protease for the maintenance of Purkinje cells dendrite and axons in adult mice, and for Purkinje cell dendritogenesis.

Hippocampal defects in *Spg7*$^{-/-}$ *Afg3l2*$^{Emv66/+}$ mice

Besides the cerebellum, histological and immunohistochemical analyses were normal in the brain of *Spg7*$^{-/-}$ *Afg3l2*$^{Emv66/+}$ mice with the exception of a small area of GFAP immunoreactivity at the end of the hippocampal fissure, suggesting recruitment of reactive glia in the stratum lacunosum-moleculare and stratum radiatum of the CA3 field (Fig. 5B). These layers contain septal and commissural fibers and perforant path fibers from the enthorinal cortex. Semithin sections showed a substantial loss of pyramidal neurons in the CA3 field (Fig. 5D), whereas neurons in the CA1 field, and granule neurons of the dentate gyrus, appeared largely normal (Fig. 5F; data not shown). These data broaden the spectrum of neurons susceptible to loss of the *m*-AAA protease in the adult brain.

Different expression levels of the *m*-AAA protease subunits in the mouse brain

The previous data suggest a different neuronal susceptibility depending on the dosage of different subunits of the *m*-AAA protease. To test whether this is due to different expression levels, we performed RNA *in situ* hybridization on adult mouse brain using probes specific for *Afg3l2*, *Afg3l1* and *Spg7*. *Afg3l2* showed a very strong pattern of expression in neurons of the brain, including all layers of the cerebral cortex, the hippocampus and the cerebellum (Fig. 6A and B). In the cerebellum, *Afg3l2* is strongly expressed in both Purkinje cells and granule cells and in neurons of the cerebellar nuclei (Fig. 6B). In contrast, *Spg7* is expressed in the cerebral cortex, the hippocampal neurons and the cerebellum at lower levels (Fig. 6C and D). Notably, in the cerebellum, *Spg7* expression appeared confined to Purkinje cells and neurons of the deep cerebellar nuclei (Fig. 6D). *Afg3l1* transcript was instead poorly detected in the brain (Fig. 6E and F). Thus, expression data support a prominent role of AFG3L2 in the brain and a cooperative role of paraplegin in hippocampal neurons and Purkinje cells.

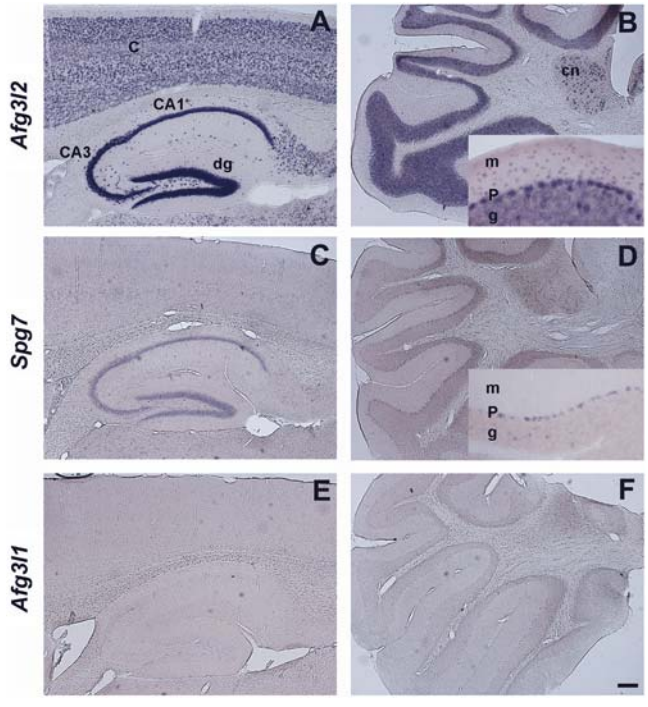

Figure 6. Differential expression of the *m*-AAA protease subunits in the brain. RNA *in situ* hybridization on sagittal brain sections using probes specific for *Afg3l2* (**A** and **B**), *Spg7* (**C** and **D**) and *Afg3l1* (**E** and **F**) shows different expression levels. The inserts show enlarged view (four times) of the Purkinje cell layer in B and D. Scale bar: 200 μm. C, cortex; dg, dentate gyrus; CA1, CA1 field; CA3, CA3 field; m, molecular layer; P, Purkinje cells; g, granule cell layer; cn, cerebellar nucleus.

Abnormal dysfunctional mitochondria in Purkinje cells of $Spg7^{-/-}$ $Afg3l2^{Emv66/+}$ mice

Ultrastructural analysis of the cerebellum in $Spg7^{-/-}$ $Afg3l2^{Emv66/+}$ mice confirmed the degenerative features of Purkinje cells with membrane blebbing and cell shrinkage and showed the accumulation of a large number of swollen degenerating mitochondria (Fig. 7B–D). These degenerating mitochondria are likely responsible for the formation of the vacuolar structures observed in semithin sections and are very similar in morphology to those already described in the spinal cord and sciatic nerve axons (Fig. 2). Abnormal mitochondria are large and have disrupted or vesicular cristae.

To evaluate the respiratory competence of these mitochondria, we performed SDH and combined COX-SDH histochemistry *in situ* on cerebellar sections. It was extremely difficult to identify Purkinje cells in sections of $Spg7^{-/-}$ $Afg3l2^{Emv66/+}$ mice processed for the histochemical reactions, even though residual atrophic Purkinje cell bodies were recognized in adjacent sections by Nissl staining (Fig. 8B, D and F). We never observed Purkinje cells negative for the COX staining but positive for SDH, consistent with the severe alteration of the mitochondria morphology in degenerating neurons (Fig. 8D). This notwithstanding, we could detect a few residual Purkinje cells still positive for both COX and SDH reaction (Fig. 8B and D), suggesting that OXPHOS impairment occurs at late stages of the degenerative process.

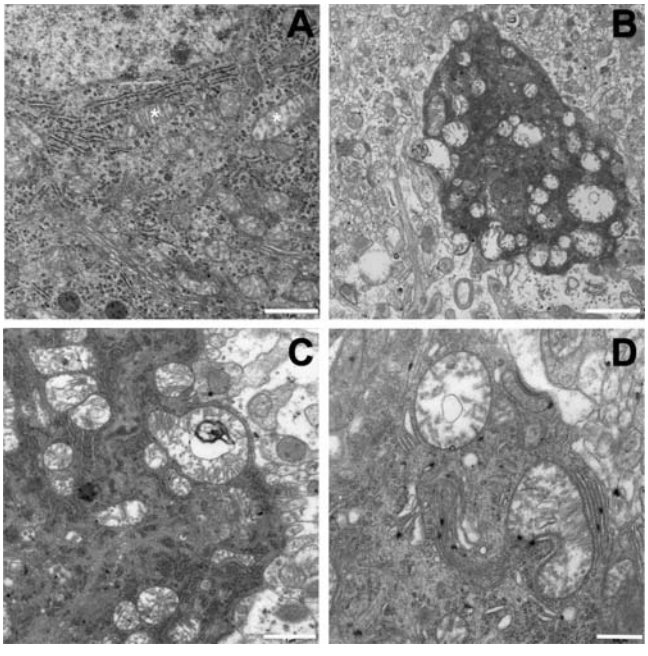

Figure 7. Mitochondrial abnormalities in Purkinje cells of $Spg7^{-/-}$ $Afg3l2^{Emv66/+}$ mice. (**A**) Electron micrographs showing the presence of normal mitochondria in the cell body of Purkinje cells in wild-type animals at 13 weeks of age. Mitochondria appear in strict proximity to the endoplasmic reticulum (A, asterisks). (**B**–**D**) In $Spg7^{-/-}$ $Afg3l2^{Emv66/+}$ mice, Purkinje cell mitochondria are abnormally swollen, with disrupted cristae. In B, a degenerated cell containing several of these abnormal mitochondria is shown. Bars: 1 μm in A and C, 5 μm in B, 500 nm in D.

The *m*-AAA protease affects mt-DNA content and stability of the respiratory complexes

We then asked whether a general molecular or biochemical defect can be unraveled in all mitochondria isolated from affected tissues. As a first step, we performed real-time PCR on total DNA extracted from the cerebellum, the forebrain and the spinal cord at 13 weeks of age. We found a statistically significant loss of mt-DNA relative to the content of nuclear DNA in the affected animals compared with wild-type littermates, especially in the cerebellum (Fig. 9A). Determination of the citrate synthase (CS) activity on whole tissue lysates to estimate the total mitochondrial mass suggested a slight tendency to decrease in the mutant mice, but appeared insufficient to account for the loss of mt-DNA (Fig. 9B).

The loss of mt-DNA is not necessarily reflected in the amount of mitochondrial respiratory complexes, as efficient compensatory mechanisms have been described both in patients and in mice with severe mt-DNA depletions (15,16). To this end, we measured specific enzymatic activities of the electron transport chain complexes spectrophotometrically in enriched mitochondria fractions from cerebellum, forebrain and spinal cord. To render respiratory complexes freely accessible to saturating concentrations of substrates in our assays, we used sonication to disrupt the outer and inner mitochondrial membranes. At 13 weeks of age, we found that the activities of complexes I, III and IV were unaffected in mitochondria isolated from $Spg7^{-/-}$ $Afg3l2^{Emv66/+}$ mice when mild conditions to disrupt membranes were applied (Supplementary Material, Fig. S6). Surprisingly, however,

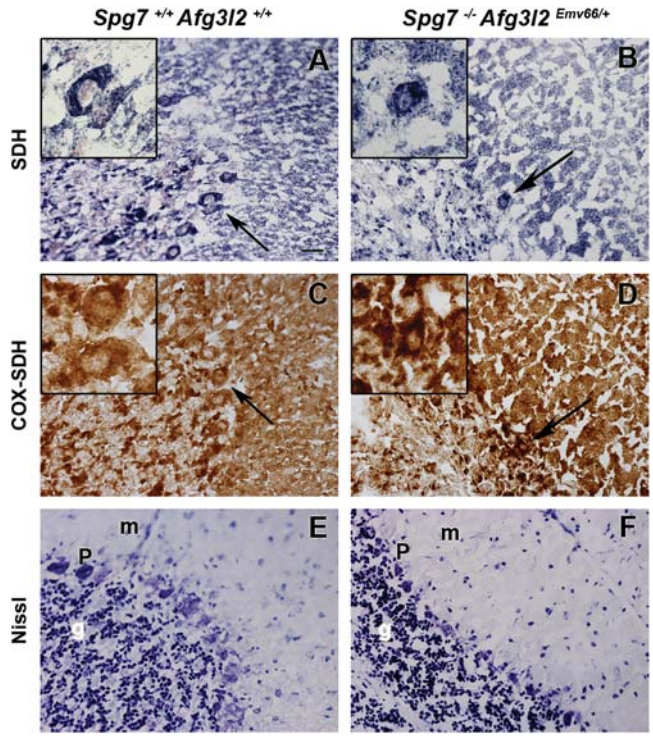

Figure 8. Purkinje cells lose COX/SDH reaction in *Spg7*$^{-/-}$ *Afg3l2*$^{Emv66/+}$ mice. Consecutive sections of the cerebellum of wild-type (**A, C** and **E**) and *Spg7*$^{-/-}$ *Afg3l2*$^{Emv66/+}$ (**B, D** and **F**) mice were subjected to SDH histochemistry, combined COX-SDH histochemistry and Nissl staining. The Purkinje cell layer is nicely stained in mice with both SDH and combined COX-SDH in wild-type mice (arrows in A and C). In contrast, reactivity is almost completely lost in *Spg7*$^{-/-}$ *Afg3l2*$^{Emv66/+}$mice. However, a few residual Purkinje cells are still positive for both COX and SDH (arrows in B and D). The inserts show high magnifications of the neurons indicated by the arrows. The Purkinje cells appear atrophic in mutant mice (F). m, molecular layer; P, Purkinje cell layer; g, granule cell layer. Scale bar: 50 μm.

we detected a statistically significant reduction ranging between 20 and 40% of the activities of complexes I, III and IV in mitochondria isolated from the spinal cord, the cerebellum and the forebrain of *Spg7*$^{-/-}$ *Afg3l2*$^{Emv66/+}$ mice, when mitochondrial fractions were subjected to longer times of sonication (Supplementary Material, Fig. S6). The activities of respiratory complexes were normal at 5 weeks of age in *Spg7*$^{-/-}$ *Afg3l2*$^{Emv66/+}$ mice, independent from the sonication regimen (data not shown). These results strongly suggest that the redox activities of the respiratory complexes are not intrinsically reduced in *Spg7*$^{-/-}$ *Afg3l2*$^{Emv66/+}$ mice, but rather point to a structural instability of the complexes.

We therefore decided to examine the stability of the assembled respiratory complexes in mitochondria with reduced dosage of the *m*-AAA protease. We used dodecylmaltoside (DDM) to allow extraction and analysis of native complexes by Blue Native gel electrophoresis (BNGE). These experiments were performed on forebrains of mice at 13 weeks of age. By using increasing ratios of detergent to total protein content, all complexes were efficiently extracted in wild-type animals. Complexes I, II and IV were stable even at high ratio of detergent to protein content, with the exception of complex III, which showed a slightly reduced stability at ratio 10 (Fig. 9C and D). In contrast, complexes I and III appeared reduced in *Spg7*$^{-/-}$ *Afg3l2*$^{Emv66/+}$ mitochondria at all DDM/protein ratios compared with controls (Fig. 9C and D). Notably, the levels of complex I were comparable in control and mutant mitochondria when using a ratio of DDM/protein of 1.5 g/g (data not shown). We found a reproducible reduction of complex IV in mitochondria of *Spg7*$^{-/-}$ *Afg3l2*$^{Emv66/+}$ mice only at a DDM/protein ratio of 10 g/g (Fig. 9C and D). In contrast, the stability of complex II was not affected even at high DDM/protein ratios (Fig. 9C and D). The steady-state levels of the individual complex subunits appeared normal by SDS–PAGE, suggesting that our results reflect the instability of the assembled complexes, rather than an increased degradation or decreased synthesis of the individual subunits (Supplementary Material, Fig. S7).

In conclusion, these results strongly suggest that the mitochondria of *Spg7*$^{-/-}$ *Afg3l2*$^{Emv66/+}$ mice have less stable respiratory complexes and tend to lose mt-DNA.

DISCUSSION

The mammalian *m*-AAA protease comprises both hetero-oligomeric paraplegin-AFG3L2 and homo-oligomeric AFG3L2 isoenzymes. Our results show strong genetic interaction between *Afg3l2* and *Spg7* in adult neurons, indicating that both *m*-AAA protease isoenzymes are required to prevent degenerative changes. Furthermore, we demonstrate for the first time that the *m*-AAA protease protects against cerebellar degeneration.

We report an early-onset severe neurological phenotype in mice that are completely devoid of paraplegin and have half dosage of AFG3L2. These mice display a drastic acceleration of the features of paraplegin-deficient mice, showing axonal degeneration in the spinal cord and sciatic nerve about 4 months earlier than in the sole absence of *Spg7* (12). Moreover, they are characterized by neurodegeneration in other selective brain areas, such as the hippocampal CA3 field and the cerebellum. Cerebellar degeneration is observed already at 7 weeks of age, is characterized by degenerative features of dendrites of Purkinje cells, by massive loss of cerebellar axons and reactive astrogliosis, and explains the main symptoms of these mice, uncoordinated movements and loss of balance. These alterations are not detected in *Spg7*$^{-/-}$, *Afg3l2*$^{Emv66/+}$ and double-heterozygous littermates at comparable ages, although we cannot exclude that mild abnormalities may arise in older animals.

Ataxia is a common symptom of mitochondrial disorders due to mutations in mt-DNA, in proteins involved in mt-DNA maintenance, and complex I components (17–19). Purkinje cell degeneration has also been recently linked to defective mitochondrial fusion (20). Remarkably, our study has important implications for human pathology. Spinocerebellar ataxia SCA28 has been mapped to the region of chromosome 18 that includes the *AFG3L2* gene in a large Italian family with a juvenile, slowly progressive, autosomal dominant form of the disease (21). Heterozygous mutations in *AFG3L2* have indeed been recently identified as the cause of SCA28 (22,23). Interestingly, one family was described in which a full-blown ataxic phenotype was evident in an

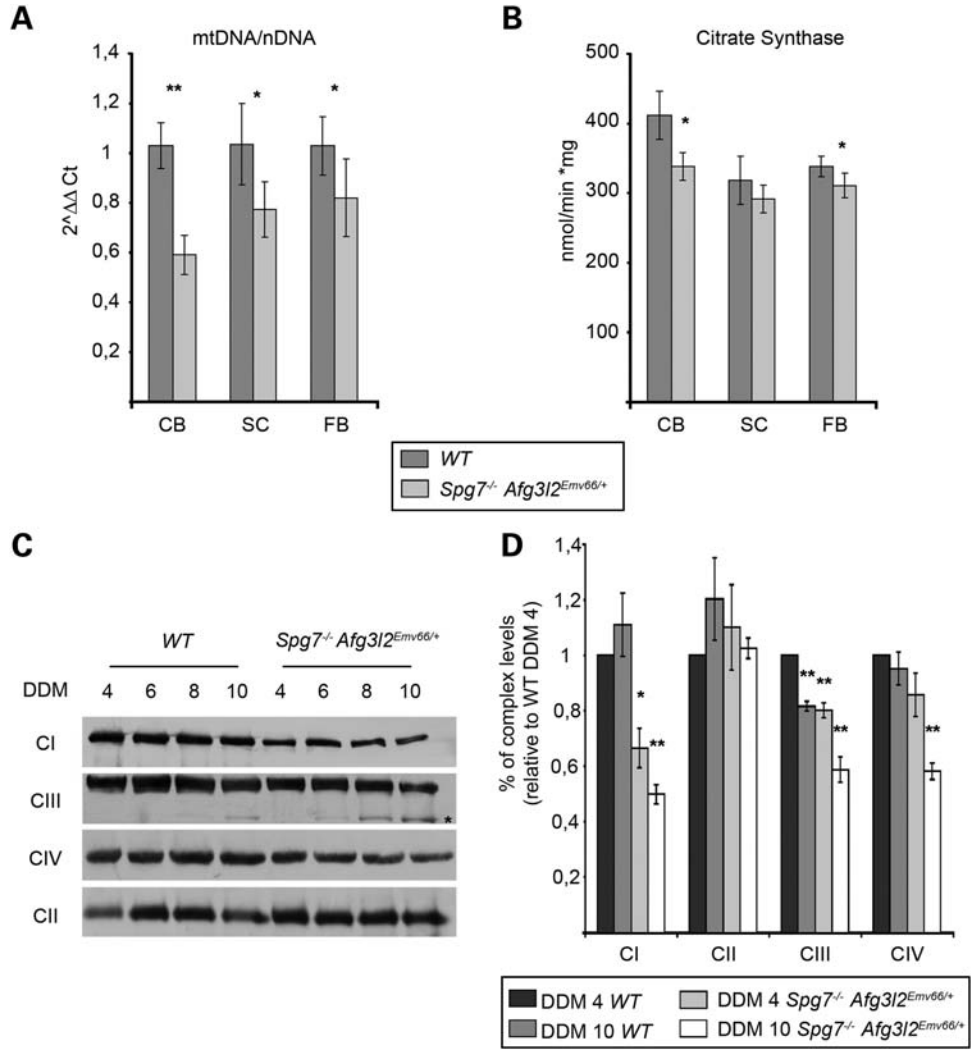

Figure 9. Biochemical analysis of $Spg7^{-/-}$ $Afg3l2^{Emv66/+}$ mitochondria. (**A**) Real-time PCR quantification reveals a statistically significant reduction of the mt-DNA content with respect to the nuclear DNA from the cerebellum (CB), the spinal cord (SC) and the forebrain (FB) of $Spg7^{-/-}$ $Afg3l2^{Emv66/+}$ mice ($n = 6$) compared with WT littermates ($n = 5$). (**B**) The mitochondrial mass estimated by measuring the enzymatic activity of the CS is not equally affected ($n = 4$ for CB and SC; $n = 6$ for FB). $^{*}P < 0.05$, $^{**}P < 0.0001$ according to Student's *t*-test. Error bars are SD. (**C**) Detection of respiratory complexes after BNGE by western blot using specific antibodies against complex I, II, III and IV. One hundred micrograms of mitochondria were solubilized with increasing concentration of DDM (shown at the top of the gel as ratio to protein content, g/g). The asterisk points to a putative degradation product of complex III. (**D**) Quantification of the levels of each complex solubilized at DDM/protein ratio 4 and 10, relative to the level of the DDM/protein ratio 4 in wild-type mitochondria. Quantification was performed on four independent experiments. $^{*}P < 0.05$, $^{**}P < 0.01$, according to Student's *t*-test (relative to WT DDM 4). Error bars are SEM.

individual who is a compound heterozygous for mutations in *AFG3L2* and *SPG7*, although mild cerebellar atrophy was reported in the *AFG3L2* heterozygous parent (23). This finding, together with our observations, clearly underlines an essential role of *AFG3L2* in preventing cerebellar degeneration and attributes an important modulatory role to paraplegin. Consistently, some overlapping features of the human phenotypes linked to these genes have been described: *SPG7*-mutated patients frequently show cerebellar symptoms (5–7), whereas SCA28 patients are often characterized by hyperreflexia at lower limbs (24).

Our study demonstrates that different neurons have variable requirements of the *m*-AAA proteases: if the loss of the hetero-oligomeric *m*-AAA protease is sufficient to cause degeneration of long murine spinal axons (12), the homo-oligomeric *m*-AAA complex must also be reduced to affect Purkinje cells. These data could be explained assuming that neurons manifest degenerative changes when the global levels of *m*-AAA proteases drop below a certain threshold. The presence in a given neuron of hetero-oligomeric versus homo-oligomeric *m*-AAA proteases can vary depending on the availability of the different subunits, thus driving the susceptibility of this neuron to loss of paraplegin and AFG3L2. Our expression data clearly indicate that the levels of each subunit of the *m*-AAA protease are very different in individual neurons. *Afg3l2* and *Spg7* are the subunits predominantly expressed in the brain. Strikingly, while *Afg3l2* is expressed at high levels in all neurons, *Spg7* shows lower levels of

expression restricted to large neurons, such as cortical and hippocampal neurons, and Purkinje cells. Notably, these are the neurons mainly affected in *Spg7*$^{-/-}$ *Afg3l2*$^{Emv66/+}$ mice, suggesting a specific role of the hetero-oligomeric complex. Our expression data further confirm that *Afg3l1* does not appear to play an important role in the brain and is therefore unlikely to compensate for the reduced levels of the other subunits in this tissue.

Mitochondria are dramatically abnormal in affected neurons and axons of *Spg7*$^{-/-}$ *Afg3l2*$^{Emv66/+}$ mice. They are prone to undergo swelling, and they show disrupted cristae, similar to what previously observed in paraplegin- and AFG3L2-deficient mice (12,13). These degenerating mitochondria ultimately lose reactivity for mitochondrial enzymes, as COX and SDH. Remarkably, general alterations are present in *Spg7*$^{-/-}$ *Afg3l2*$^{Emv66/+}$ brain and spinal cord mitochondria, which tend to lose mt-DNA and display reduced levels of assembled respiratory complexes, especially of complexes I, III and IV, at high detergent/protein ratio. Decreased levels of assembled complex I and III were also found previously in the brain of *Ag3l2*$^{Emv66/Emv66}$ mice (13). This notwithstanding, the steady-state levels of the components of the respiratory complexes and the intrinsic activities of the complexes are largely normal, strongly suggesting instability rather than reduced assembly of the complexes. It is worth of note that the affected complexes are those containing more subunits inserted into the inner mitochondrial membrane. Instability of respiratory complexes could also explain the puzzling finding of an impairment of their specific activities only when harsher conditions are used to disrupt mitochondrial membranes. Interestingly, an old study has already described a peculiar sensitivity of complex IV to sonication in skeletal muscle biopsies from patients with various OXPHOS diseases (25). The hypothesis of a decreased stability of respiratory complexes may explain the variability of complex I deficiency in cell lines obtained from different patients with *SPG7* mutations, depending on the technique used (7,26).

A possible explanation for the mitochondrial alterations may be an age-dependent accumulation in mitochondria of misfolded polypeptides altering membrane properties. Another possibility is that this phenotype may depend on impaired maturation of specific substrates. The only known substrate of both yeast and mammalian *m*-AAA protease is the ribosomal component MrpL32 (11). We found that mitochondria isolated from the cerebellum of *Spg7*$^{-/-}$ *Afg3l2*$^{Emv66/+}$ mice display slightly reduced levels of mature MrpL32 and an accumulation of its precursor to a variable extent (data not shown). Although the amount of processed MrpL32 is sufficient to allow normal synthesis of respiratory complex subunits, we cannot exclude a specific role in Purkinje cells. Furthermore, other yet unknown substrates of the *m*-AAA protease may contribute to the mitochondrial dysfunction specifically in these cells. Proteins involved in nucleoid stability, mt-DNA maintenance, lipid content of the membrane may be considered attractive candidates.

In conclusion, we provide evidence for an important role of the homo-oligomeric AFG3L2 *m*-AAA complex in neuronal degeneration, establish neuronal-specific redundant functions of the homo-oligomeric and hetero-oligomeric isoenzymes and point to the cerebellum as a novel target for neuronal degeneration due to impaired mitochondrial proteolysis. Our data strongly support the view that mechanisms that underlie degeneration of long central and peripheral axons may intersect with those underlying Purkinje cell degeneration. Owing to their extremely long axons, or to their remarkable dendritic tree, these neurons can be a preferential target when mitochondrial dynamics, transport and function are even slightly perturbed.

MATERIALS AND METHODS

Mouse management

All animal procedures were performed according to protocols approved by the Institutional Animal Care and Use Committee. Generation of *Spg7*$^{-/-}$ mice (12) and *Afg3l2*$^{Emv66/Emv66}$ genetic characterization (13) were described previously. *Spg7*$^{-/-}$ mice (on a mixed C57BL6-129Sv background) were bred with *Afg3l2*$^{+/Emv66}$ mice (FVB background). Double-heterozygous mice obtained by this breeding were further intercrossed to obtain mice with different dosages of *Spg7* and *Ag3l2*. All experiments were conducted on littermates derived from this last breeding. The genotype of mice was identified by PCR using specific primers. Primer sequences are available upon request.

Phenotype characterization

Mice were weighed starting from 3 weeks of age ($n \geq 7$ animals for each genotype). Motor performance was evaluated with a Rota-Rod apparatus (accelerating model; Ugo Basile, Varese, Italy). Groups of *WT* ($n = 8$), *Spg7*$^{-/-}$ ($n = 7$) and age-matched *Spg7*$^{-/-}$ *Afg3l2*$^{Emv66/+}$ ($n = 16$) were analyzed at 5, 7 and 9 weeks of age. Before the first test, mice were trained on the rotarod for 60 s at 4 rpm at constant speed. For the tests, mice were placed on the accelerating rod at a starting speed of 4 rpm, reaching a final speed of 40 rpm in 300 s. Mice were tested for two trials at 20 min intervals for 3 consecutive days. The animals were allowed to stay on the rod for a maximum of 300 s and their time on the rod was recorded. Statistical analysis was performed using Student's *t*-test for each trial.

Histology and immunohistological analyses

Animals were anesthetized with avertin and perfused intracardially with 4% paraformaldehyde in PBS. Cerebella were removed, post-fixed overnight with 4% paraformaldehyde in PBS and conserved in 0.12 M phosphate buffer. Immunohistochemistry and immunofluorescence were performed on 30 μm sagittal vibratome sections. Briefly, free-floating sections were pre-treated for 30 min in sucrose 4%/PBS and for 30 min in methanol. Immunohistochemistry for phosphorylated neurofilament and GFAP were performed on sections permeabilized and blocked in 0.5% Triton X-100, 10% goat serum in PBS. SMI31 (1:3000, Covance Research Products, Berkeley, CA, USA) and anti-GFAP (0.5 μg/ml, NeoMarkers, Fremont, CA, USA) primary antibodies were incubated overnight in a solution containing 0.5% Triton X-100, 5% goat serum in

PBS. Biotinylated anti-mouse IgG antibody (Vector Lab, Burlingame, CA, USA) was incubated in 5% goat serum in PBS. Detection was performed using the Vectastain®-ABC kit (Vector Lab), as specified by the manufacturer. Immunofluorescence for calbindin was performed on sections permeabilized in 0.5% Triton X-100, 20% goat serum in TBS solution. The monoclonal anti-calbindin antibody (Swant, Bellinzona, Switzerland) was used overnight (1:1500) in 0.5% Triton X-100, 10% goat serum in TBS. AlexaFluor 488 and 546 anti-mouse IgG antibodies (Invitrogen, Carlsbad, CA, USA) were incubated in 10% goat serum in TBS. All immunohistochemical and immunofluorescence analyses were performed on at least five mice per genotype.

Neuropathology and electron microscopy

Semithin and ultrathin morphological analyses were conducted as described (27,28). Age-matched wild-type, *Spg7*$^{-/-}$ and *Spg7*$^{-/-}$ *Afg3l2*$^{Emv66/+}$ mice ($n = 3$ for each genotype) were anesthetized intraperitoneally with avertin and perfused with 4% paraformaldehyde in PBS. The spinal cord, sciatic nerve and cerebellum were removed and postfixed in 0.12 M phosphate buffer/2% glutaraldehyde. They were then postfixed with osmium tetroxide and embedded in Epon (Fluka, Buchs SG, Switzerland). Cross-sections were cut from the lumbar spinal cord and sciatic nerve, whereas the cerebellum was cut sagittally. For ultrastructural analyses, blocks of tissue were selected for electron microscopy after light microscopy examination of semithin sections.

Morphometry

All morphometric analyses were performed in a blinded and unbiased manner. Purkinje cells counts were performed on 30 μm sagittal vibratome sections stained with Nissl solution. We counted the total number of Purkinje cells with an evident nucleus in lobule III of the cerebellum. At least two independent sections for three animals/genotype were scored. To quantify the number of Purkinje cells with degenerative features, we performed morphometry on semithin sections by scoring the number of Purkinje cells with abnormal morphology and vacuoles in the cytoplasm ($n = 3$ per genotype). Ultrastructural morphometric analyses were performed on photographs captured using an electron microscope. For all mice, non-overlapping photographs were taken from the lumbar columns and sciatic nerve.

RNA *in situ* hybridization

To obtain specific probes for *in situ* hybridization, fragments of the mouse *Afg3l2* (nucleotides 2199–2870), *Spg7* (nucleotides 175–1146) and *Afg3l1* (nucleotides 47–831) cDNAs were subcloned and used as templates to transcribe either sense or antisense digoxygenin-labeled riboprobes using the DIG RNA labeling kit (Roche). Vibratome sections were permeabilized with proteinase K 10 μg/ml for 10 min. *In situ* hybridization was performed essentially as described previously (29).

Histochemical staining

Cryostat sections (10 μm thick) were collected on SuperFrost®Plus coverslips (Menzel-Glaser, Portsmouth, New Hampshire, USA). Sections were incubated in SDH solution (0.1 M succinic acid disodium salt, 0.1 M phosphate buffer, 2.5 mM nitrobluetetraziolium) for 90 min at 37°C in a humid chamber. For combined COX-SDH staining, sections were incubated first with COX solution (3,3′-diaminobenzidine 5.5 mM, cytocrome C 165 mM, sucrose 220 mM, catalase 2 mg/ml in phosphate buffer 0.05 M) for 15 min at 37°C in a humid chamber, washed in PBS and then incubated in SDH solution as described earlier. Sections were washed in PBS and fixed in PFA 4% in PBS.

Mitochondria isolation

The dissected tissues were promptly chopped and homogenized (10 strokes) with 10 volumes/g wet tissue of MOPS sucrose buffer (440 mM sucrose, 20 mM Mops, 1 mM EDTA, 0.2 mM phenylmethylsulphonyl fluoride) in a glass-Teflon pestle. The crude homogenate was centrifuged at 500*g* for 10 min at 4°C. The low-speed supernatant was centrifuged at 10 000*g* for 10 min at 4°C. The resulting mitochondrial pellet was carefully resuspended in MOPS sucrose buffer and centrifuged at 10 000*g* for 10 min at 4°C. The final mitochondrial pellet was resuspended to 10–20 mg/ml in MOPS sucrose buffer. Protein concentration was determined by Bradford's method (BioRad, Hercules, CA, USA) with BSA as the standard.

Blue Native polyacrylamide gel electrophoresis

BNGE was performed essentially as described previously (30). Briefly, 100 μg of mitochondria were solubilized for 10 min in 20 μl of 1 M ε-amino *n*-caproic acid, 50 mM Tris (pH 7.0) and increasing concentration of DDM (detergent-to-protein ratio were 4, 6, 8 or 10 g/g). Insoluble material was removed by centrifugation at 20 000*g* for 90 min at 4°C. The supernatant was collected and combined with Serva blue G (5% in 1 M ε-amino *n*-caproic acid). The amount of Serva blue G added was calculated to give a detergent/dye ratio of 4 (g/g). The respiratory chain complexes were separated on a gradient gel of 5–13% acrylamide in 150 mM Bis-Tris, 1.5 mM ε-amino *n*-caproic acid adjusted to pH 7.0. The cathode buffer (50 mM Tricine, 15 mM Bis-Tris/HCl, pH 7.0, and 0.02% Serva blue G) was used until the dye front had reached approximately a half of the way through the gel before exchange with colorless cathode buffer. The anode buffer was 50 mM Bis–Tris/HCl, pH 7.0. Native complex was separated at 300 V and 12 mA for 3 h at 4°C.

Western blot analysis

For immunodetection of the respiratory complexes after BNGE, the following antibodies were used: 39 kDa subunit of complex I, 70 kDa subunit of complex II, core II subunit of complex III, subunit I and Vb of complex IV (Invitrogen). Quantification was performed using Quantity One (BioRad) on four independent western blots.

Real-time quantification of mt-DNA

Total DNA was isolated from the cerebellum and the spinal cord by standard techniques. Real-time amplification was performed using SYBR® Green PCR Master Mix (Applied Biosystem, Foster City, CA, USA) in an ABI PRISM 7000 Sequence Detection System. Primers for mt-DNA were located on murine COI gene (31), and primers for murine RNase-P were used as nuclear gene standard reference. Primer sequences are available upon request. Each PCR reaction was performed in triplicate with the following profile: one cycle at 50°C for 2 min, one cycle at 95°C for 10 min and then 40 cycles at 95°C for 15 s and 60°C for 1 min (two-step protocol).

CS activity

The dissected tissues were promptly chopped and homogenized (10 strokes) with 10 volumes/g wet tissue of isolation buffer (220 mM D-mannitol, 70 mM sucrose, 20 mM HEPES, 1 mM EDTA and 0.1% BSA, pH 7.2) in a glass-Teflon pestle. The crude homogenate was centrifuged at 500*g* for 10 min. The low-speed supernatant was collected. CS activity was determined spectrophotometrically at 30°C. To completely remove the permeability barrier for substrates, samples were freezed–thawed and sonicated for 15 s twice at 40 W before use. CS activity was determined as the reduction rate of 100 μM DTNB (5,5′-dithio-bis-2-nitrobenzoic acid) at 412 nm ($\varepsilon = 13.8\ \text{mM}^{-1}\ \text{cm}^{-1}$), after the addition of 400 μM acetyl-coenzyme A and 100 μM oxalacetate. All reagents employed for biochemical analyses were from Sigma-Aldrich (St Louis, MO, USA).

SUPPLEMENTARY MATERIAL

Supplementary Material is available at *HMG* online.

ACKNOWLEDGEMENTS

The authors wish to thank Thomas Langer for many fruitful discussions, Valeria Tiranti for critical reading of the manuscript and Giorgia Dina for technical assistance.

Conflict of Interest statement: None declared.

FUNDING

This work has been supported by grants from the UMDF, the MDA and the CARIPLO foundations to E.I.R., and from FIRB and Istituto Superiore Sanità to A.Q.

REFERENCES

1. Beal, M.F. (2005) Mitochondria take center stage in aging and neurodegeneration. *Ann. Neurol.*, **58**, 495–505.
2. Lin, M.T. and Beal, M.F. (2006) Mitochondrial dysfunction and oxidative stress in neurodegenerative diseases. *Nature*, **443**, 787–795.
3. Harding, A.E. (1983) Classification of the hereditary ataxias and paraplegias. *Lancet*, **321**, 1151–1154.
4. Fink, J.K. (2006) Hereditary spastic paraplegia. *Curr. Neurol. Neurosci. Rep.*, **6**, 65–76.
5. Casari, G., De Fusco, M., Ciarmatori, S., Zeviani, M., Mora, M., Fernandez, P., De Michele, G., Filla, A., Cocozza, S., Marconi, R. *et al.* (1998) Spastic paraplegia and OXPHOS impairment caused by mutations in paraplegin, a nuclear-encoded mitochondrial metalloprotease. *Cell*, **93**, 973–983.
6. Elleuch, N., Depienne, C., Benomar, A., Hernandez, A.M., Ferrer, X., Fontaine, B., Grid, D., Tallaksen, C.M., Zemmouri, R., Stevanin, G. *et al.* (2006) Mutation analysis of the paraplegin gene (SPG7) in patients with hereditary spastic paraplegia. *Neurology*, **66**, 654–659.
7. Arnoldi, A., Tonelli, A., Crippa, F., Villani, G., Pacelli, C., Sironi, M., Pozzoli, U., D'Angelo, M.G., Meola, G., Martinuzzi, A. *et al.* (2008) A clinical, genetic, and biochemical characterization of SPG7 mutations in a large cohort of patients with hereditary spastic paraplegia. *Hum. Mutat.*, **29**, 522–531.
8. Koppen, M., Metodiev, M.D., Casari, G., Rugarli, E.I. and Langer, T. (2007) Variable and tissue-specific subunit composition of mitochondrial m-AAA protease complexes linked to hereditary spastic paraplegia. *Mol. Cell. Biol.*, **27**, 758–767.
9. Kremmidiotis, G., Gardner, A.E., Settasatian, C., Savoia, A., Sutherland, G.R. and Callen, D.F. (2001) Molecular and functional analyses of the human and mouse genes encoding AFG3L1, a mitochondrial metalloprotease homologous to the human spastic paraplegia protein. *Genomics*, **76**, 58–65.
10. Rugarli, E.I. and Langer, T. (2006) Translating m-AAA protease function in mitochondria to hereditary spastic paraplegia. *Trends Mol. Med.*, **12**, 262–269.
11. Nolden, M., Ehses, S., Koppen, M., Bernacchia, A., Rugarli, E.I. and Langer, T. (2005) The m-AAA protease defective in hereditary spastic paraplegia controls ribosome assembly in mitochondria. *Cell*, **123**, 277–289.
12. Ferreirinha, F., Quattrini, A., Pirozzi, M., Valsecchi, V., Dina, G., Broccoli, V., Auricchio, A., Piemonte, F., Tozzi, G., Gaeta, L. *et al.* (2004) Axonal degeneration in paraplegin-deficient mice is associated with abnormal mitochondria and impairment of axonal transport. *J. Clin. Invest.*, **113**, 231–242.
13. Maltecca, F., Aghaie, A., Schroeder, D.G., Cassina, L., Taylor, B.A., Phillips, S.J., Malaguti, M., Previtali, S., Guenet, J.L., Quattrini, A. *et al.* (2008) The mitochondrial protease AFG3L2 is essential for axonal development. *J. Neurosci.*, **28**, 2827–2836.
14. Armengol, J.A. and Sotelo, C. (1991) Early dendritic development of Purkinje cells in the rat cerebellum. A light and electron microscopic study using axonal tracing in 'in vitro' slices. *Brain Res. Dev. Brain Res.*, **64**, 95–114.
15. Viscomi, C., Spinazzola, A., Maggioni, M., Fernandez-Vizarra, E., Massa, V., Pagano, C., Vettor, R., Mora, M. and Zeviani, M. (2009) Early-onset liver mtDNA depletion and late-onset proteinuric nephropathy in Mpv17 knockout mice. *Hum. Mol. Genet.*, **18**, 12–26.
16. Barthelemy, C., Ogier de Baulny, H., Diaz, J., Cheval, M.A., Frachon, P., Romero, N., Goutieres, F., Fardeau, M. and Lombes, A. (2001) Late-onset mitochondrial DNA depletion: DNA copy number, multiple deletions, and compensation. *Ann. Neurol.*, **49**, 607–617.
17. Zeviani, M., Antozzi, C., Savoiardo, M. and Bertini, E. (2002) Ataxia in mitochondrial disorders. In Manto, M.U. and Pandolfo, M. (eds), *The Cerebellum and Its Disorders*. Cambridge University Press, pp. 548–561.
18. Hakonen, A.H., Goffart, S., Marjavaara, S., Paetau, A., Cooper, H., Mattila, K., Lampinen, M., Sajantila, A., Lonnqvist, T., Spelbrink, J.N. *et al.* (2008) Infantile-onset spinocerebellar ataxia and mitochondrial recessive ataxia syndrome are associated with neuronal complex I defect and mtDNA depletion. *Hum. Mol. Genet.*, **17**, 3822–3835.
19. Kruse, S.E., Watt, W.C., Marcinek, D.J., Kapur, R.P., Schenkman, K.A. and Palmiter, R.D. (2008) Mice with mitochondrial complex I deficiency develop a fatal encephalomyopathy. *Cell Metab.*, **7**, 312–320.
20. Chen, H., McCaffery, J.M. and Chan, D.C. (2007) Mitochondrial fusion protects against neurodegeneration in the cerebellum. *Cell*, **130**, 548–562.
21. Cagnoli, C., Mariotti, C., Taroni, F., Seri, M., Brussino, A., Michielotto, C., Grisoli, M., Di Bella, D., Migone, N., Gellera, C. *et al.* (2006) SCA28, a novel form of autosomal dominant cerebellar ataxia on chromosome 18p11.22–q11.2. *Brain*, **129**, 235–242.
22. Cagnoli, C., Stevanin, G., Durr, A., Ribai, P., Forlani, S., Brussino, A., Pappi, P., Pugliese, L., Barberis, M., Margolis, R.L. *et al.* (2008) Mutations in AFG3L2 gene (SCA28) in autosomal dominant cerebellar ataxias. *Annual Meeting of the American Society of Human Genetics*, Philadelphia, Pennsylvania.

23. DiBella, D., Lazzaro, F., Brusco, A., Battaglia, G., Pastore, A., Finardi, A., Fracasso, V., Plumari, M., Cagnoli, C., Tempia, F. *et al.* (2008) AFG3L2 mutations cause autosomal dominant ataxia SCA28 and reveal an essential role of the m-AAA AFG3L2 homocomplex in the cerebellum. *Annual Meeting of the American Society of Human Genetics*, Philadelphia, Pennsylvania.
24. Mariotti, C., Brusco, A., Di Bella, D., Cagnoli, C., Seri, M., Gellera, C., Di Donato, S. and Taroni, F. (2008) Spinocerebellar ataxia type 28: a novel autosomal dominant cerebellar ataxia characterized by slow progression and ophthalmoparesis. *Cerebellum*, **7**, 184–188.
25. Zheng, X.X., Shoffner, J.M., Voljavec, A.S. and Wallace, D.C. (1990) Evaluation of procedures for assaying oxidative phosphorylation enzyme activities in mitochondrial myopathy muscle biopsies. *Biochim. Biophys. Acta*, **1019**, 1–10.
26. Atorino, L., Silvestri, L., Koppen, M., Cassina, L., Ballabio, A., Marconi, R., Langer, T. and Casari, G. (2003) Loss of m-AAA protease in mitochondria causes complex I deficiency and increased sensitivity to oxidative stress in hereditary spastic paraplegia. *J. Cell. Biol.*, **163**, 777–787.
27. Previtali, S.C., Quattrini, A., Fasolini, M., Panzeri, M.C., Villa, A., Filbin, M.T., Li, W., Chiu, S.Y., Messing, A., Wrabetz, L. *et al.* (2000) Epitope-tagged P(0) glycoprotein causes Charcot–Marie–Tooth-like neuropathy in transgenic mice. *J. Cell Biol.*, **151**, 1035–1046.
28. Consiglio, A., Quattrini, A., Martino, S., Bensadoun, J.C., Dolcetta, D., Trojani, A., Benaglia, G., Marchesini, S., Cestari, V., Oliverio, A. *et al.* (2001) *In vivo* gene therapy of metachromatic leukodystrophy by lentiviral vectors: correction of neuropathology and protection against learning impairments in affected mice. *Nat. Med.*, **7**, 310–316.
29. Tiveron, M.C., Hirsch, M.R. and Brunet, J.F. (1996) The expression pattern of the transcription factor Phox2 delineates synaptic pathways of the autonomic nervous system. *J. Neurosci.*, **16**, 7649–7660.
30. Nijtmans, L.G., Henderson, N.S. and Holt, I.J. (2002) Blue Native electrophoresis to study mitochondrial and other protein complexes. *Methods*, **26**, 327–334.
31. Spinazzola, A., Viscomi, C., Fernandez-Vizarra, E., Carrara, F., D'Adamo, P., Calvo, S., Marsano, R.M., Donnini, C., Weiher, H., Strisciuglio, P. *et al.* (2006) MPV17 encodes an inner mitochondrial membrane protein and is mutated in infantile hepatic mitochondrial DNA depletion. *Nat. Genet.*, **38**, 570–575.